Hindawi
Geofluids
Volume 2021, Article ID 1747705, 14 pages
https://doi.org/10.1155/2021/1747705

Research Article

Remote Sensing of Atmospheric CO and O_3 Anomalies before and after Two Yutian M_S7.3 Earthquakes

Haodong Liang, Cunlin Xin, Haibo Liu, Guoyun Di, Songxin Liu, and Liang Zhang

College of Geography and Environmental Science, Northwest Normal University, Lanzhou 730000, China

Correspondence should be addressed to Cunlin Xin; xincunling@163.com

Received 2 May 2021; Revised 4 August 2021; Accepted 14 August 2021; Published 1 September 2021

Academic Editor: Orlando Vaselli

Satellite remote sensing data were used to extract concentrations and volume mixing ratios (VMR) of CO and O_3 and Global Data Assimilation System (GDAS) data associated with Yutian M_S7.3 earthquakes on March 21, 2008, and February 12, 2014. Difference value and anomaly index methods and the Hybrid Single-Particle Lagrangian Integrated Trajectory (HYSPLIT) model were used to simulate gas backward trajectories and analyze the relations between spatial and temporal variations in total columns of CO and O_3 (TotCO and TotO_3) and earthquakes. Then, the causes of abnormal changes were examined. Maximum anomalies in TotCO and TotO_3 occurred one month before the 2008 earthquake and one month after the 2014 earthquake. Anomalies in TotCO and TotO_3 were distributed along or were consistent with the fault zone. Furthermore, during the abnormal period, the coefficient of correlation between CO and O_3 was 0.672 in 2008 and 0.638 in 2014, with both values significant at $p < 0.05$. The correlation between TotCO and TotO_3 was also significant. The abnormal phenomena of TotCO and TotO_3 associated with the two earthquakes were attributed to underground gas escape, atmospheric chemical reactions, and atmospheric transportation caused by in situ stress in the generation of earthquakes.

1. Introduction

Understanding earthquake precursory anomalies is a worldwide concern [1]. At present, ground observations based on geophysics and crustal deformation are the typical focus of research [2]. However, it is difficult to obtain large-area dynamic and continuous information on seismic precursory anomalies because of limitations in ground observations, which restrict the ability to predict earthquakes [1]. Satellite hyperspectral technology has the advantages of wide coverage and short observation period and is not affected by the underlying surface [2]. The technology can identify different gases, invert their concentration distributions, and predict earthquakes [3]. With the development of satellite remote sensing technology, using abnormal changes in gas concentrations near epicenters to predict earthquakes has become a focus of research [4, 5]. However, the mechanisms for the abnormal changes remain unclear because of a lack of research. The C–H–O–S system of the earth is rich and includes CO_2, CH_4, H_2, CO, O_3, water vapor, and other gases [6–8]. These gases escape to the atmosphere from seismic fault and rupture zones before and after earthquakes and thus can change atmospheric composition and concentrations [9–12]. After the Gujarat M_S7.7 (2001) and M_S5.2 (2006) earthquakes, high-altitude O_3-rich air was transported to the epicenter area by the atmosphere, which increased its O_3 concentration [13]. Similarly, before and after two $M_S >$ 8.0 earthquakes in Sumatra in 2004 and 2005, abnormal changes were detected in CO and O_3 concentrations, primarily caused by escape of underground gases during the earthquake and chemical reactions between underground and atmospheric gases [14]. Before and after the Wenchuan M_S8.0 earthquake in 2008 and the Lushan M_S7.0 earthquake in 2013, there were abnormal spatiotemporal changes in CH_4 and CO, and Cui et al. [15] proposed that they were caused by the two major earthquakes and the accompanying fault tectonic activities. Similarly, Singh et al. [16] suggest that abnormal change in CO concentration before the Gujarat

M_S7.7 earthquake in India in 2010 was precursor information on the earthquake. Thus, satellite hyperspectral remote sensing data can be used in seismic monitoring.

The Yutian 2008 M_S7.3 earthquake (35.6°N, 81.6°E) occurred in Yutian, Xinjiang, China, at 0633 on March 21, 2008, with a focal depth of 19 km. The earthquake rupture was primarily extensional and strike-slip, and the epicenter was the intersection of the Kangxiwa fault zone and the southwest end of the Arerjin fault zone in the West Kunlun Mountains. The main seismogenic fault structure is the Arerjin fault [17]. Before this earthquake, there were two $M_S \geq 6$ (excluding aftershocks) earthquakes within 500 km of the 2008 Yutian earthquake epicenter. One was a 6.1 earthquake in Rutog County, Tibet, on May 5, 2007 (140 km from the 2008 Yutian earthquake epicenter), and the other was a 6.9 earthquake in Gêrzê County, Tibet, on January 9, 2008 (480 km from the 2008 Yutian earthquake epicenter). Since then, the extension of the fault zone in the region has increased. On August 12, 2012, another M_S6.2 earthquake occurred 90 km from the 2008 Yutian earthquake, resulting in long-term crustal instability and accumulation of strain energy in the region. As a consequence, a M_S7.3 earthquake (36.1°N, 82.5°E) occurred at 1719 on February 12, 2014, in Yutian, Xinjiang. The focal depth of the 2014 Yutian earthquake was 12 km, and the mechanism was a strike-slip type. The tail of the large strike-slip Arerjin fault zone, which is an extension zone in the southwest section of the fault zone, was the epicenter. Atmospheric infrared sounder (AIRS) data were obtained, and the difference and anomaly index methods were used to analyze temporal and spatial variations in O_3 and CO gases before and after two earthquakes. The relations and the differences between the two earthquakes were also examined. Figure 1 shows the faults and seismic history of the research area.

2. Data and Methods

2.1. Data. Column concentration data of CO, O_3, and CH_4 (TotCO, TotO_3, and TotCH_4) and volume mixing ratio data of CO and O_3 (VMR) were all derived from the 8-day data, monthly average standard product deorbit data, and daily data of the AIRS level 3 of the National Aeronautics and Space Administration (NASA). The data were downloaded from NASA's Goddard Earth Sciences Data and Information Services Center (http://disc.sci.gsfc.nasa.gov/). The 2008 Yutian earthquake epicenter area was 35.6°N, and the average value of a gas was that in a 1° × 1° space at 81.6°E. The 2014 Yutian earthquake epicenter area was 36.1°N, and the average value of a gas was that in a 1° × 1° space at 82.5°E. For spatial distributions, gas concentrations were determined from 33°N to 39°N and 79°E to 85°E. Because AIRX3STD data (AIRS+AMSU) were used in this paper, sensor data were only available to 2016. Therefore, data from 2003 to 2015 were used. The AIRS is a hyperspectral sensor mounted on the Aqua satellite launched by NASA on May 4, 2002. The satellite can cover 85% of the earth twice a day. The AIRS has 2,378 continuous infrared spectral channels, which can provide hyperspectral resolution data in the wavelength range from 3.7 to 15.4 μm with a spatial resolution of 1° × 1°. The spectral resolution was $\lambda/D\lambda > 1{,}200$ nominal. It can monitor the physical parameters pressure, temperature, and humidity and the chemicals CH_4, CO, and O_3 [18, 19]. The meteorological data used for backward trajectory were from atmospheric assimilation products and model reanalysis data of the National Centers for Environmental Prediction (NCEP) in the US and were obtained through the GDAS, which assimilates a variety of conventional data and satellite observation data. The data set included air temperature, humidity, near-surface wind speed, and near-surface pressure, with a time resolution of 3 h and a spatial resolution of 1° × 1°. The data were downloaded from the official website of the NCEP of the National Meteorological Administration (https://www.noaa.gov/ [20]).

2.2. Methods. Data were extracted by MATLAB, and the abnormal index method and the difference method were used to subtract the average value of the gas background field in nonseismic years and eliminate the influence of seasonal changes. The HYSPLIT model was used to examine transport and diffusion trajectories of O_3.

(1) Extraction of CO, CH_4, and O_3 data. The CO, CH_4, and O_3 concentration data and the VMR data were in NASA standard disk storage format HDF-type (hierarchical data format). MATLAB (2021a) software was used to extract the data, and ArcGIS (10.5) software was used for interpolation processing.

(2) Abnormal index method. This method is similar to the definition of thermal anomaly [21, 22], and the A_{index} (equation (2)) is the ratio of the difference (equation (3)) to the standard deviation ($\sigma(x, y, t)$) (equation (1)) [15]. The anomaly index is used to assess the reliability of anomalies. When the $A_{\text{index}} > 2$, the anomaly reliability reaches 95.44%.

(3) Difference method. This method directly reflects the absolute variation in a gas by using the abnormal difference value and highlighting the abnormal degree by which a gas concentration value deviates from the background value. The anomaly difference is the difference between the current gas concentration ($G(x, y, t)$) and the background gas concentration ($G_{\text{bac}}(x, y, t)$) at one point. The monthly background value G_{bac} was the average value of each month corresponding to the nonearthquake years from 2003 to 2015 and was obtained using equation (4). [15]

$$\sigma(x, y, t) = \text{sqrt}\left\{\sum_{i=1}^{N}\left[G_i(x, y, t) - \frac{G_{\text{bac}}(x, y, t)]^2}{N-1}\right)\right\}, \quad (1)$$

$$A_{\text{index}}(x, y, t) = \frac{A(x, y, t)}{\sigma(x, y, t)}, \quad (2)$$

$$A(x, y, t) = G(x, y, t) - G_{\text{bac}}(x, y, t), \quad (3)$$

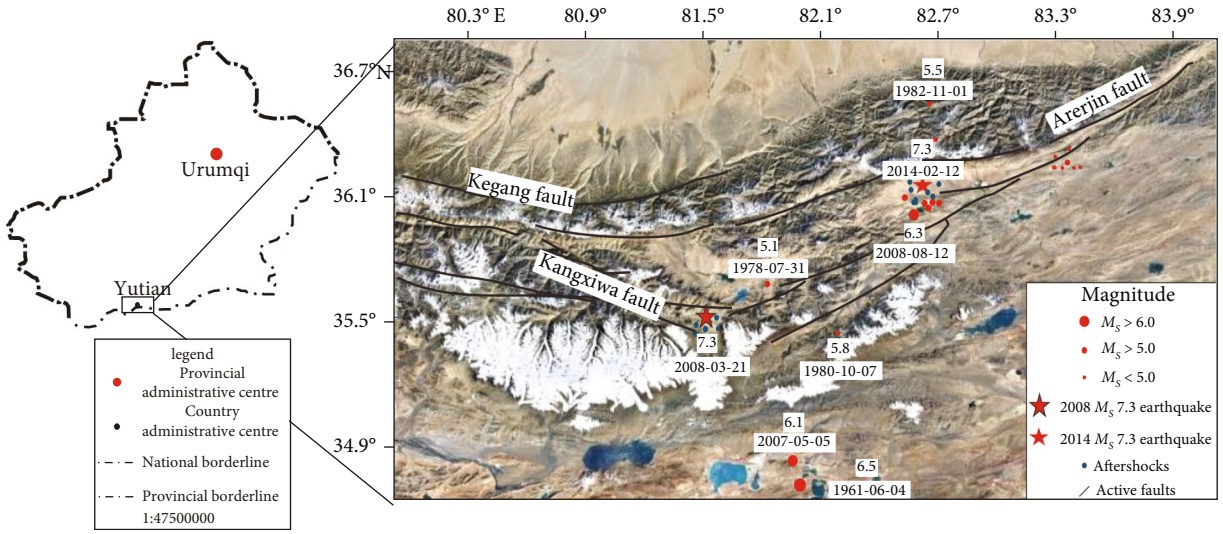

Figure 1: The geomorphologic image of the Yutian M_S7.3 research region [25].

$$G_{\text{bac}}(x, y, t) = \sum_{i=1}^{N} \frac{G_i(x, y, t)}{N}. \quad (4)$$

In the formulas, x, y, and t are the longitude, latitude, and month, respectively; G is the gas column concentration value at the current point (longitude x, latitude y) in month t; and G_{bac} is, for the time in N years ($N = 13$, 2003 to 2015), the arithmetic mean value of the gas column concentration at the same point (longitude x, latitude y) in month t. The value $\sigma(x, y, t)$ is the standard deviation at the point (longitude x, latitude y) in month t.

(4) HYSPLIT model

The HYSPLIT model is a professional model used to calculate and analyze transport and diffusion trajectory of atmospheric pollutants [23]. The model has two primary forms: backward transport and forward diffusion. Of the two, backward simulation is another form of simulating the flow direction of the target area and has been primarily used to explain the gas source in a target area [23, 24]. In this paper, HYSPLIT backward trajectory was used to simulate the transmission path of O_3 on the day of an earthquake and the maximum concentration day, as well as the O_3 contribution rate to the air mass.

3. Results

Characteristics of TotCO and $TotO_3$ anomalies associated with the two M_S7.3 earthquakes in Yutian in 2008 and 2014 obtained by difference value and anomaly index methods are shown in Table 1.

3.1. Spatial Anomaly Features. The difference method indicated the anomaly of TotCO before the 2008 Yutian earthquake that occurred primarily in the northwest direction of the epicenter, appearing along the NWW (west-northwest) trending the Tekrick fault (Figure 2(a)). The results obtained by the anomaly index method were similar to those obtained by the difference method, and the maximum anomaly index was 2.0σ (Figure 2(b)). The results indicated that it might be associated with the 2008 Yutian earthquake. Figure 3(a) shows that $TotO_3$ anomalies before the 2008 Yutian earthquake were primarily distributed in a double ring, with the line between the extreme value centers of the two abnormal rings stretching in an EW direction. The distribution of abnormal bands shown in Figure 3(b) was consistent with that in Figure 3(a), and the maximum anomaly index was approximately 2.2σ.

Figure 4(a) shows that the TotCO anomaly was linearly distributed in the NE (northeast) direction along the Arerjin fault-Xiaoerkule-Ashe Cooley fault after the 2014 Yutian earthquake. The CO anomaly distribution in Figure 4(b) was generally consistent with that in Figure 4(a), with a maximum anomaly index of approximately 1.97σ. However, the TotCO anomaly shown in Figure 4(b) was slightly weaker than that in Figure 4(a). Figure 5(a) shows that the anomalous concentration of $TotO_3$ after the 2014 Yutian earthquake was linear along the Ashkule-Guozhacuo fault zone. Similar results are shown in Figure 5(b), with an anomaly index of approximately 2.0σ. Theoretically, the anomaly centers of TotCO and $TotO_3$ should be near the epicentral fault zone and overlap each other. However, this expectation was not supported by the results, possibly because of the topographic conditions and the gas distribution height in Yutian County. Yutian County is ox leg-shaped, with the terrain higher in the south and lower in the north, with a height difference of approximately 3,500 m. The Kashtash and Kunlun mountains are in the south of Yutian County, and the Taklimakan Desert and the Tarim Basin are in the north. The CO was concentrated primarily near the surface. A downdraft prevails in the basin, and a pressure difference develops between the basin and the alpine region, forming a local atmospheric circulation that moves the CO release point northward to form an abnormal center. O_3 was concentrated primarily at high altitudes, where wind speeds

Table 1: Characteristics of atmospheric CO and O_3 anomalies associated with the Yutian M_S7.3 earthquakes on March 21, 2008, and February 12, 2014.

		2008 Yutian M_S7.3 earthquake			2014 Yutian M_S7.3 earthquake		
	Method	Time	Spatial	Maximum anomalous amplitude	Time	Spatial	Maximum anomalous amplitude
CO anomalous characteristics	A	Feb	Extension along the NWW direction consistent with the fault zone	1.01×10^{17}	Mar	Linear distribution along the NE fault zone	1.17×10^{17}
	A_{index}	Feb	Extension along the NWW direction consistent with the fault zone	2.0	Mar	Double annular extremum and stretching along the NE direction	1.97
O_3 anomalous characteristics	A	Feb	Double annular extremum and stretching along the EW direction	22.67	Mar	Linear distribution along the NE fault zone	31.71
	A_{index}	Feb	Double annular extremum and stretching along the EW direction	2.2	Mar	Linear distribution along the NE fault zone	2.18

Note: A represents the difference method; A_{index} represents the abnormal index method; the unit of the abnormal amplitude of CO is molecules/cm^2; the unit of the abnormal amplitude of O_3 is DU.

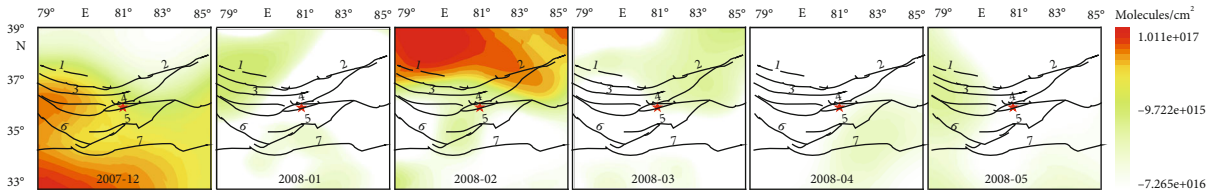

(a) Spatial distribution of CO anomalies obtained by the difference method

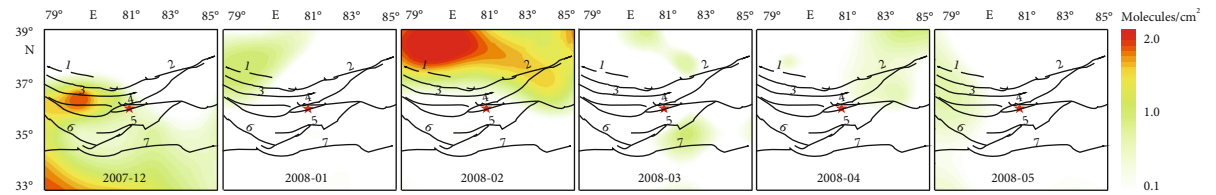

(b) Spatial distribution of CO anomalies obtained by the anomaly index method

Figure 2: Spatial distribution of CO concentration anomalies (molecules/cm^2) before and after the Yutian earthquake on March 21, 2008. 1—Tekrick fracture; 2—Arerjin fracture; 3—Kangxiwa fracture; 4—Yulong Kashi fracture; 5—Guozhacuo fracture; 6—Tianshen Daban fracture; and 7—Longmucuo-Bangdacuo fracture. Red five-pointed star indicates the epicenter location.

are high and gas flow is fast. Affected by northerly wind, O_3 moves southward from the original release point to form an abnormal center [26]. Therefore, the TotCO and TotO_3 anomaly centers shifted and did not coincide with one another.

3.2. Temporal Anomaly Characteristics. The maximum anomalies of TotCO and TotO_3 occurred one month before the 2008 Yutian earthquake (Figures 2 and 3). A small-amplitude CO concentration anomaly occurred in December 2007 (Figure 2), which might be associated with the 6.9-magnitude earthquake in Gêrzê County, Tibet, on January 9, 2008 (480 km from the epicenter of the 2008 Yutian earthquake) [27]. Then, the maximum TotCO anomaly appeared in February and gradually recovered to a 5normal level of variation from March. The timing of anomalous change in TotO_3 (Figure 3) was generally consistent with that of TotCO. As shown in Figure 6(a), TotCO increased sharply from February 8, reached its maximum on February 10, and then decreased gradually. The TotCO also increased from February 28 to March 13, but the change in amplitude was small, consistent with periodic changes. After that increase, the TotCO returned to the level of periodic change. The TotO_3 began to increase from February 8, breaking the cycle of gradual change, but then decreased sharply on February 11 (Figure 6(a)). Then, TotO_3 began to increase sharply on February 23 and reached a maximum on February 27. After the maximum, TotO_3 decreased and returned to a cycle of gradual change. The VMR values of CO and O_3 at 700 hPa from 2003 to February 2015 were extracted

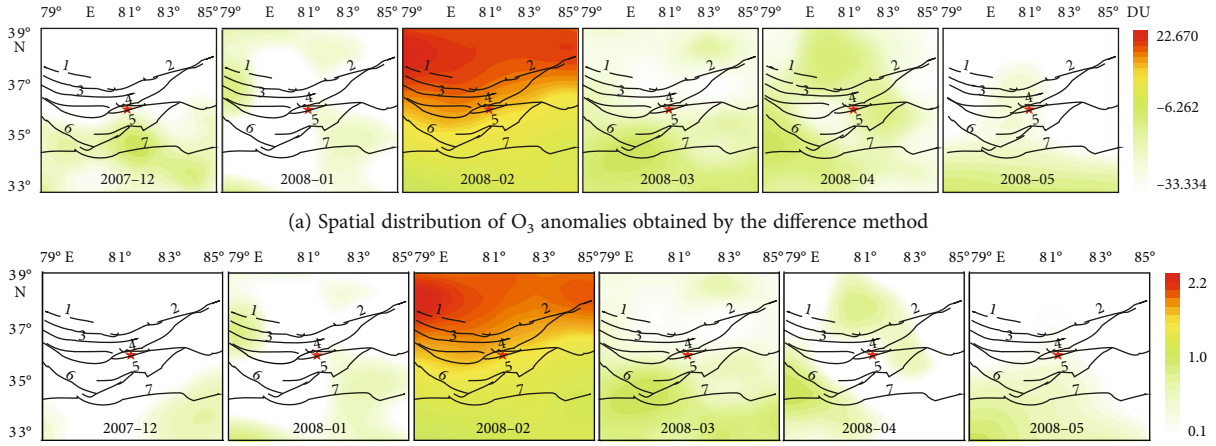

(a) Spatial distribution of O_3 anomalies obtained by the difference method

(b) Spatial distribution of O_3 anomalies obtained by the anomaly index method

Figure 3: Spatial distribution of O_3 concentration anomalies (molecules/cm^2) before and after the Yutian earthquake on March 21, 2008. 1—Tekrick fracture; 2—Arerjin fracture; 3—Kangxiwa fracture; 4—Yulong Kashi fracture; 5—Guozhacuo fracture; 6—Tianshen Daban fracture; and 7—Longmucuo-Bangdacuo fracture. Red five-pointed star indicates the epicenter location.

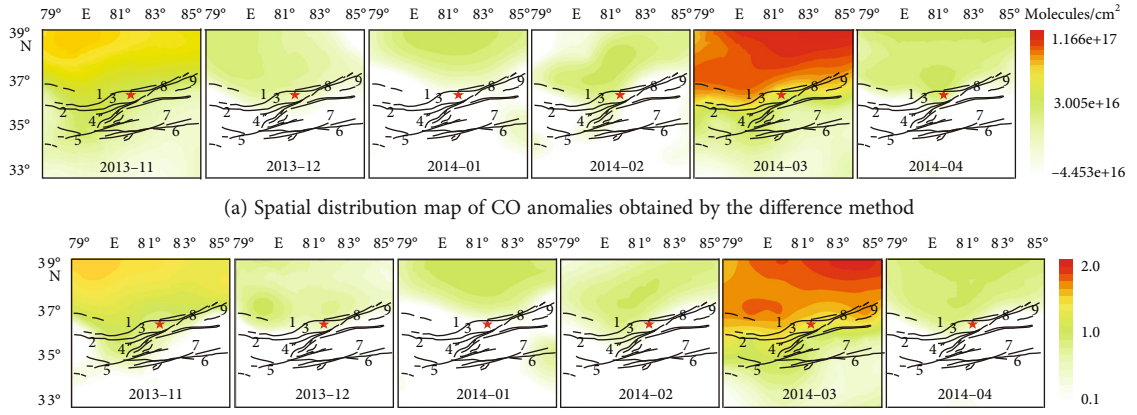

(a) Spatial distribution map of CO anomalies obtained by the difference method

(b) Spatial distribution map of CO anomalies obtained by the anomaly index method

Figure 4: Spatial distribution of CO concentration anomalies before and after the Yutian earthquake on February 12, 2014. 1—Peru fracture; 2—Ashe Cooley-Xiaoerkule fracture; 3—Kangxiwa fracture; 4—Kuyake fracture; 5—Guozhacuo fracture; 6—Longmucuo-Bangdacuo fracture; 7—Margai Caka fracture; 8—Gonggacuo fracture; and 9—Arerjin fracture. Red five-pointed star indicates the epicenter location.

and analyzed, and the values increased sharply at the beginning of February 2008, around February 4 (Figure 7(a)). Maximum values were reached on February 22, 2008. By contrast, in other nonseismic years, the VMR values of CO and O_3 did not change significantly. These results indicated that the abnormal changes in TotCO and TotO_3 in February 2008 were not seasonal. Thus, the cause of those changes was most likely associated with the earthquake.

The CO VMR values at 400 to 700 hPa increased significantly from January 5 to February 22 (Figure 8(a)). The CO VMR values increased rapidly above 600 hPa and reached a maximum value on February 22. Then, the values began to decline and returned to normal levels of annual change in April. The CO VMR values at 100 to 300 hPa also increased, but the changes were not obvious because of the height. The O_3 VMR values at 300 hPa, 100 hPa, and 150 hPa increased on December 28, 2007 (Figure 9(a)). The O_3 VMR value at 300 hPa reached a maximum on March 15, whereas at 100 hPa and 150 hPa, maximum values were reached on January 15. Among the pressure layers, the changes in O_3 VMR values were most obvious at 100 hPa and 300 hPa, which may be related to the main distribution height of O_3 in the atmosphere. The changes in TotCO and TotO_3 and VMR values were consistent whether they were obtained by the difference method or the abnormal index method.

The TotCO changed slightly in November 2013 (Figure 4), and the TotO_3 changed abnormally in December 2013 (Figure 5), which may be associated with the M_S5.6 earthquake (36.8°N, 86.7°E) that occurred on November 24, 2013. Afterward, TotCO and TotO_3 increased gradually, and the maximum anomalies appeared in March 2014. As shown in Figure 6(b), TotO_3 increased sharply on March 1, 2014, and reached a maximum on March 5. From March 5 to 11, TotO_3 was higher than that in other months. There

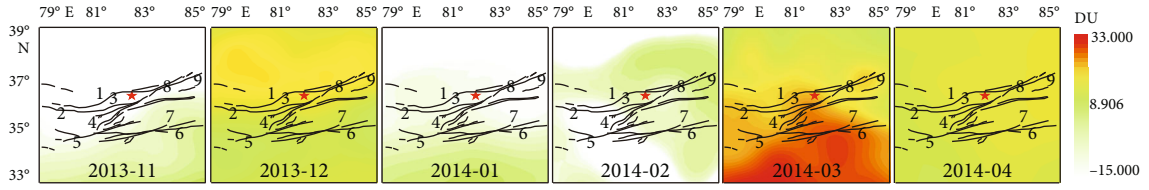

(a) Spatial distribution map of CO anomalies obtained by the difference method

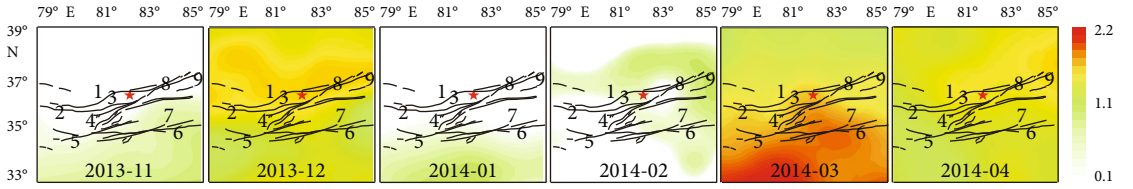

(b) Spatial distribution map of CO anomalies obtained by the anomaly index method

Figure 5: Spatial distribution of CO concentration anomalies before and after the Yutian earthquake on February 12, 2014. 1—Peru fracture; 2—Ashe Cooley-Xiaoerkule fracture; 3—Kangxiwa fracture; 4—Kuyake fracture; 5—Guozhacuo fracture; 6—Longmucuo-Bangdacuo fracture; 7—Margai Caka fracture; 8—Gonggacuo fracture; and 9—Arerjin fracture. Red five-pointed star indicates the epicenter location.

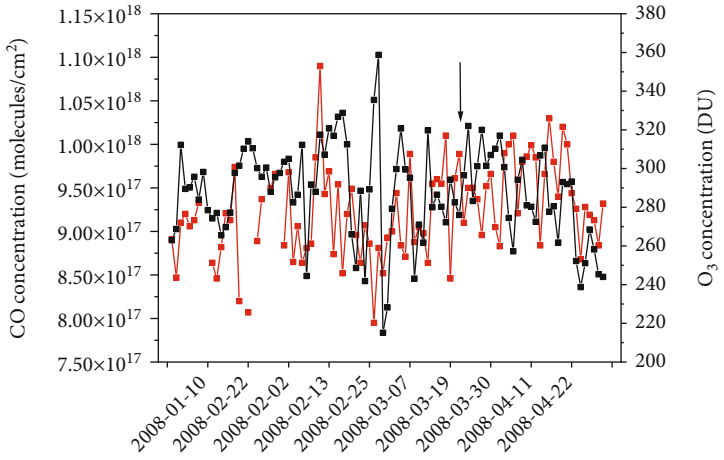

(a) Changes in gas concentrations from January to April 2008

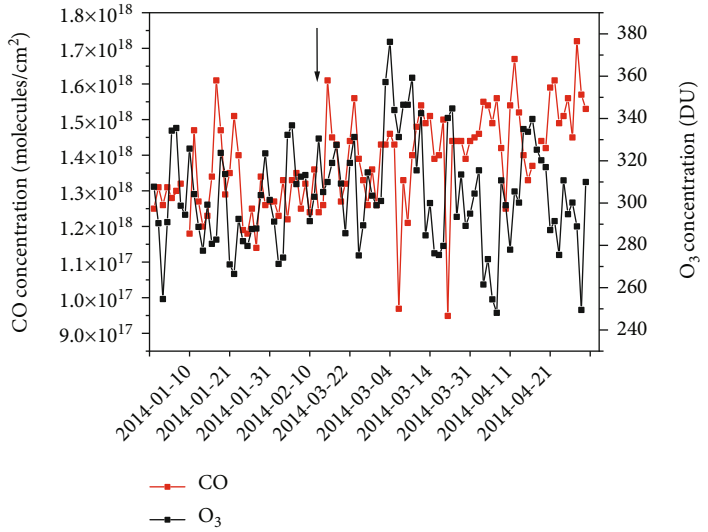

(b) Changes in gas concentrations from January to April 2014

Figure 6: Changes in CO (molecules/cm^2) and O_3 (DU) concentrations in the Yutian earthquake epicenter areas from January to April in 2008 and 2014. Arrows indicate earthquake dates.

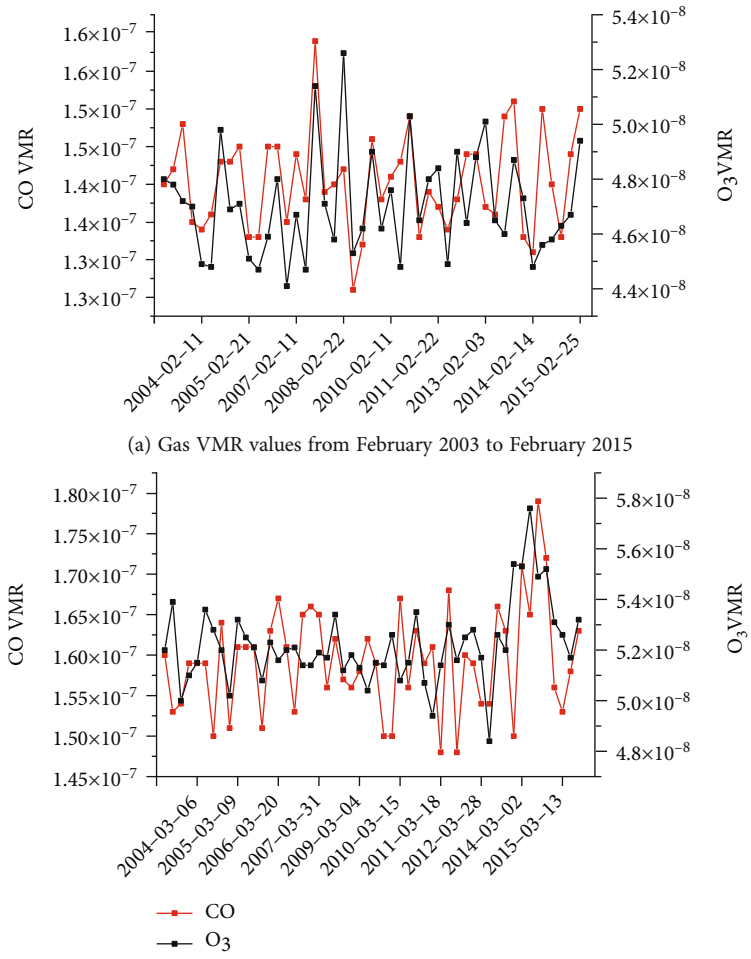

(a) Gas VMR values from February 2003 to February 2015

(b) Gas VMR values from March 2003 to March 2015

FIGURE 7: Variations in volume mixing ratio (VMR) values of CO and O_3 gases at 700 hPa during two M_S7.3 earthquakes in Yutian from February 2003 to March 2015.

were two minimum values of TotCO on March 6 and March 20, which might have been caused by the northward drift of CO from the epicenter. This result indicated that the abnormal change in TotCO might be associated with the 2014 Yutian earthquake. As shown in Figure 7(b), the VMR value of CO began to increase sharply in early March 2014, peaked around March 20, 2014, and then declined and gradually returned to normal at the end of March. The O_3 VMR also began to increase sharply in early March 2014 and reached a maximum on March 10, 2014. Then, the values began to decline and gradually returned to normal at the end of March. There were no abnormal changes in CO and O_3 VMR values in March in nonseismic years. Thus, the abnormal changes in CO and O_3 VMR values in March 2014 were not related to seasonal changes and therefore were likely associated with the 2014 Yutian earthquake. As shown in Figure 8(b), the 850 hPa CO VMR value increased sharply after February 14th, reached a maximum value on March 10–18, and then began to decline. The 400 to 700 hPa CO VMR values also showed upward trends, but the magnitude of increase was small. Maximum values were reached around March 10, which then returned to normal levels in May. These results demonstrated that changes in the 400 to 850 hPa CO VMR values were because of contributions from near the ground. As shown in Figure 9(b), the O_3 VMR values at 300 hPa, 100 hPa, and 150 hPa gradually increased after November 18, 2013. The O_3 VMR values at 300 hPa began to increase on March 1 and reached a maximum before and after March 25. The O_3 VMR values at 100 hPa and 150 hPa reached a maximum around March 1, indicating that the increase in O_3 VMR values did not necessarily come from the near surface but might have come from atmospheric chemical reactions and atmospheric transport [28].

4. Discussion

4.1. Relations between TotCO and TotO$_3$ Anomalies and Earthquakes. The TotCO was abnormal three months before the 2008 Yutian earthquake and reached the maximum abnormality in February before that earthquake. The maximum abnormal value of TotCO occurred on February 10, and the degree of abnormality exceeded the background value of 1.011×10^{17} molecules/cm^2 (Figure 2(a)). Then,

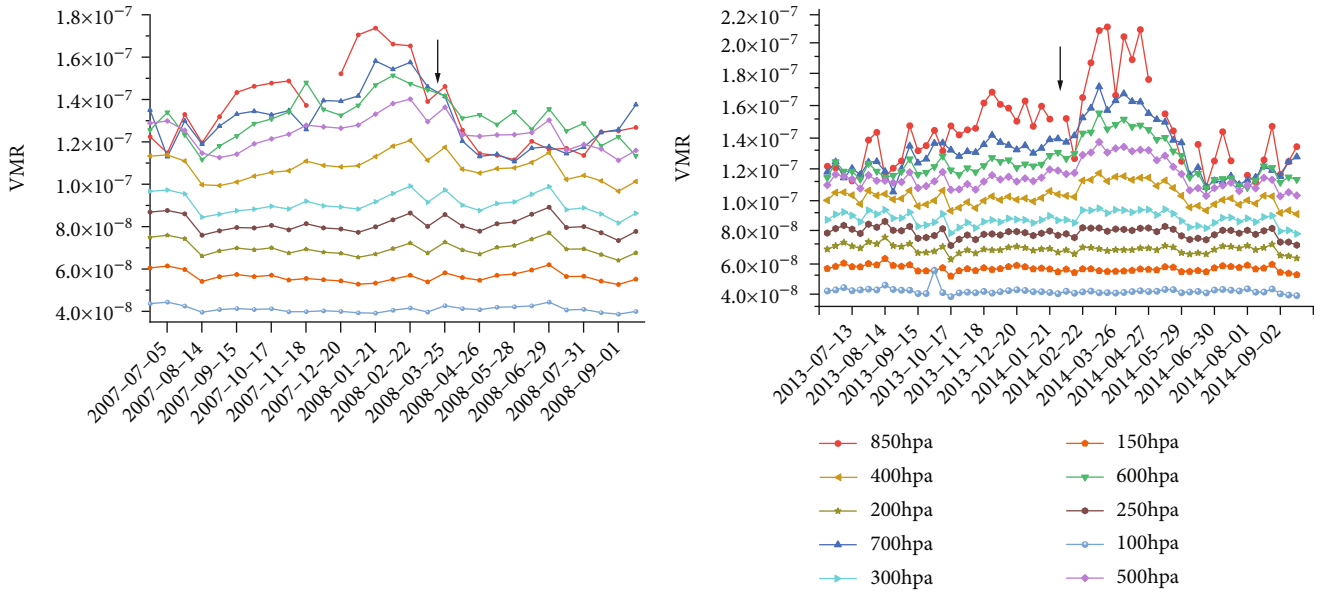

(a) 2008 Yutian earthquake

(b) 2014 Yutian earthquake

FIGURE 8: Changes in CO volume mixing ratio (VMR) values at different heights before and after two M_S7.3 Yutian earthquakes. Arrows indicate earthquake dates.

TotCO decreased abnormally and gradually returned to the level of periodic changes. During the abnormal period, the abnormal fluctuation range of TotCO was large at first and then small from the beginning of February 2008. In the month of the 2008 Yutian earthquake, TotCO also fluctuated, but the range of fluctuation was smaller than that in February (Figure 6(a)), which might be related to changes in underground gas emissions caused by changes in ground stress during earthquake buildup. In addition, TotCO showed a slight abnormality three months before the 2014 Yutian earthquake and then returned to normal, which might be associated with an M_S5.6 earthquake (36.8°N, 86.7°E) that occurred on November 24, 2013. In March 2014, TotCO reached the maximum abnormality, and the maximum abnormal value exceeded the background value of 1.166×10^{17} molecules/cm^2 during the same period, after which the abnormal degree of TotCO decreased. This result might be related to the release of ground stress during the earthquake in this area, which caused the fault zone near the epicenter to close before the earthquake and then open afterward. As shown in Figure 6(b), there were two extremely low TotCO values on March 6 and March 20. The low values might be because the gas in the epicenter area was evacuated to the northern area far from the epicenter under the influence of atmospheric circulation. This phenomenon was consistent with the results in Figure 4, which further illustrated that abnormal changes in TotCO might be associated with the 2014 Yutian earthquake.

The $TotO_3$ was abnormal one month before the earthquake on March 21, 2008. The maximum abnormal value of $TotO_3$ occurred on February 27, exceeding the background value of 22.67 DU during the same period. Then, the variation in values returned to normal (Figure 3(a)). In addition, $TotO_3$ began to appear abnormal two months before the earthquake on February 12, 2014, and reached the maximum abnormality in March 2014. The maximum abnormal value of $TotO_3$ occurred on March 5, exceeding the background value of 33 DU during the same period (Figure 5(a)), and then, the degree of abnormality decreased. The abnormal values of $TotO_3$ appeared later than those of TotCO, and their duration was longer than that of CO. The spatial correspondence of the two was relatively good, but their intensities were not consistent. The differences might be related to the multiple causes of O_3 abnormalities. In addition to underground gas escape and atmospheric chemical reactions, atmospheric transportation might also affect $TotO_3$ abnormalities. Moreover, the spatial distributions of the anomaly centers of $TotO_3$ and TotCO in 2014 did not correspond well (Figures 4 and 5) which might be related to the topography and gas distribution height in Yutian County.

In the past two decades, the strong earthquakes on the Qinghai-Tibet Plateau have generally been distributed on the periphery of the Bayan Har Block [29]. The 2008 Yutian earthquake occurred on the western boundary of the Bayan Har Block. Wan et al. [29] studied the regional structure of the fault zone around the 2008 Yutian earthquake. They found that under the NNE thrust of the Indian Plate against the Eurasian Plate, the Qaidam Basin in the northern margin of the Qinghai-Tibet Plateau moved eastward along the Arerjin fault, whereas the Xingdukush block moved NW along the Karakorum fault as a whole. The epicenter area was between the two blocks, resulting in slow, large-scale strain accumulation in the crust of the epicenter area. The EW-trending tension of the fault zone before the earthquake occurred under the bilateral dynamic interaction, and when

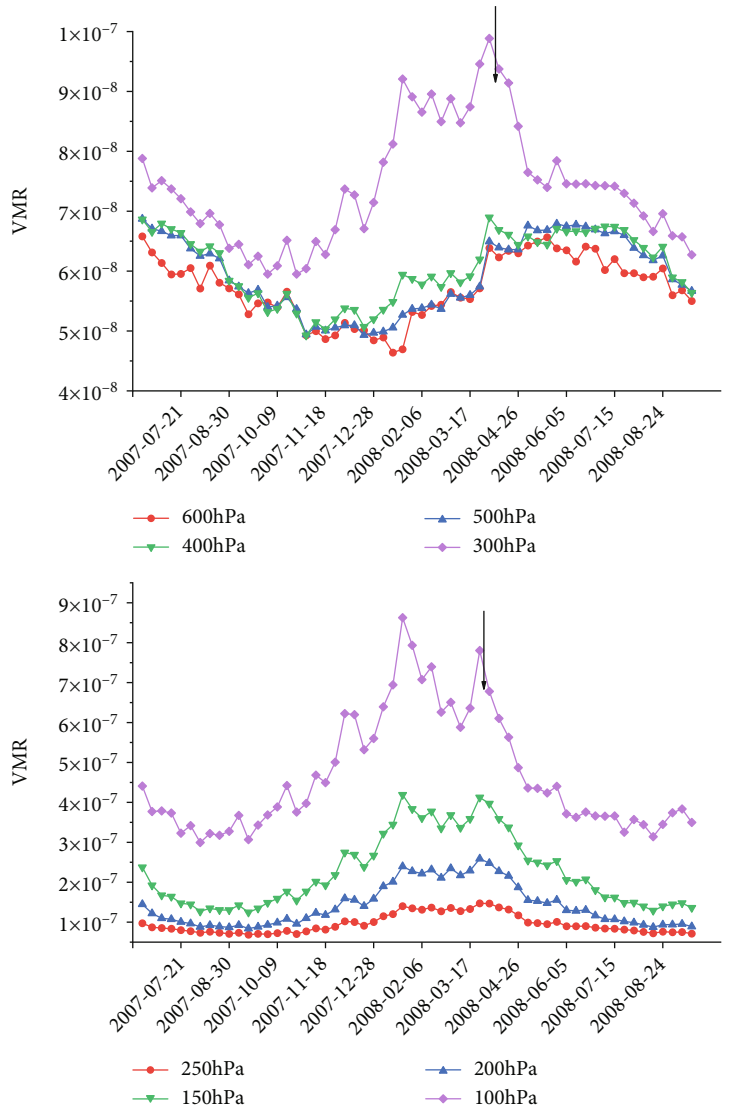

(a) 2008 Yutian earthquake

Figure 9: Continued.

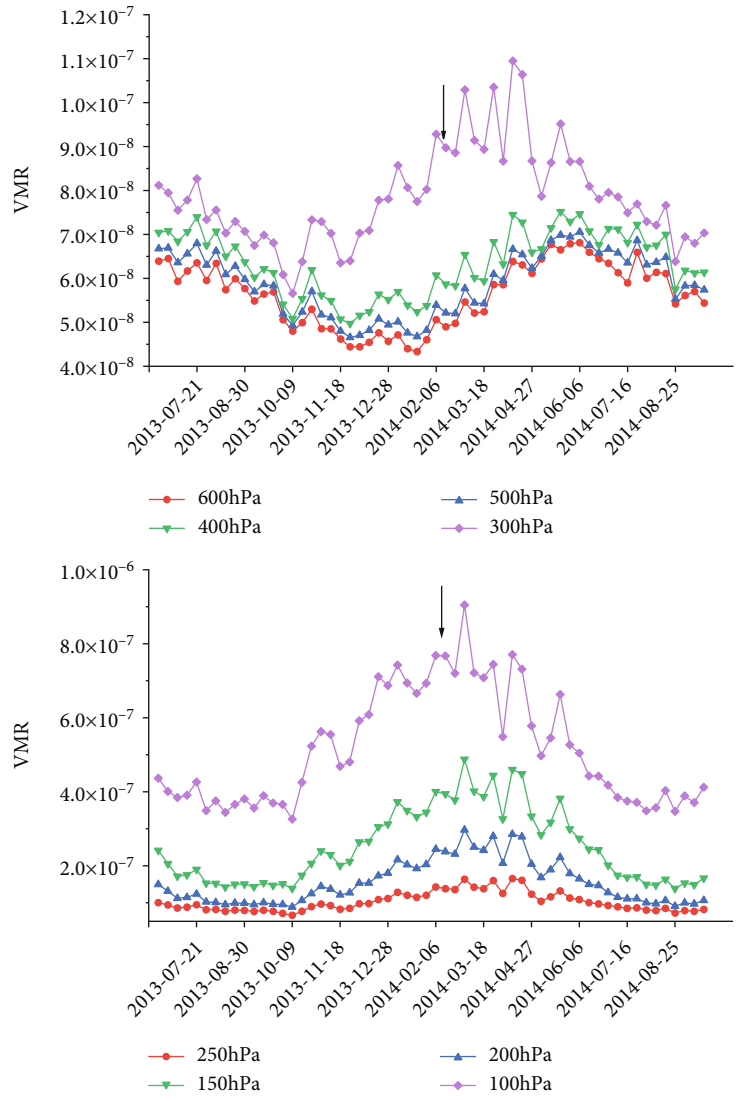

(b) 2014 Yutian earthquake

Figure 9: Changes in CO volume mixing ratio (VMR) values at different heights before and after two M_S7.3 Yutian earthquakes. Arrows indicate earthquake dates.

the structure was unlocked, the in situ stress was released. The authors speculated that underground gas was released in large quantities, resulting in anomalies. After the earthquake, the structure was locked, and the anomaly gradually decreased. Afterward, the coseismic stress disturbance of the 2008 Yutian earthquake [27] triggered subsequent aftershocks and the M_S6.2 earthquake (90 km from the 2008 Yutian earthquake epicenter) that occurred on August 12, 2012. As a result, stress increased on the Kunlun fault in the northern segment of the Gonggacuo fault zone [29], such that the southwestern end of the Arerjin fault expanded along the NW tensile structural belt [30], which accelerated the 2014 Yutian earthquake. Because of the tectonic stress caused by the 2008 Yutian earthquake and its triggered aftershocks, the Xiaoerkule fault and the Ashe Cooley fault were locked before the earthquake. Therefore, the gas upward flow pores were closed, resulting in a decrease in normal overflow gas in the short term before and after the earthquake and a continuous decline in gas concentration. After the earthquake, the stress in this area was released. The tectonic stress of the Arerjin fault resulted in the SN-trending rupture of the Xiaoerkule Basin, which accelerated the sinistral dislocation of the Arerjin fault and formed a series of NE or NNE-trending plume fault systems, including the Ashe Cooley fault and the Guozhacuo fault. The underground

Table 2: Coefficients of correlation between CO, O_3, and CH_4 gas concentrations associated with two M_S7.3 earthquakes in Yutian.

Gases	Year					
	2007	2008	2009	2013	2014	2015
CO, O_3	0.317	0.672	0.017	0.300	0.638	0.359
CH_4, CO	-0.112	-0.731	-0.378	-0.288	-0.370	-0.264
CH_4, O_3	-0.394	-0.660	-0.034	-0.342	-0.558	-0.404

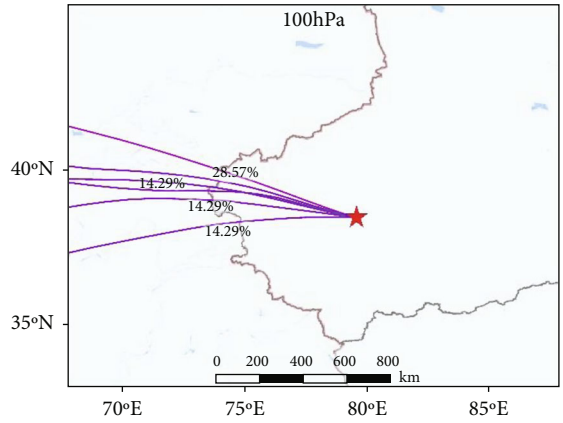

(a) Five-day backward trajectories on the day of the earthquake (March 21)

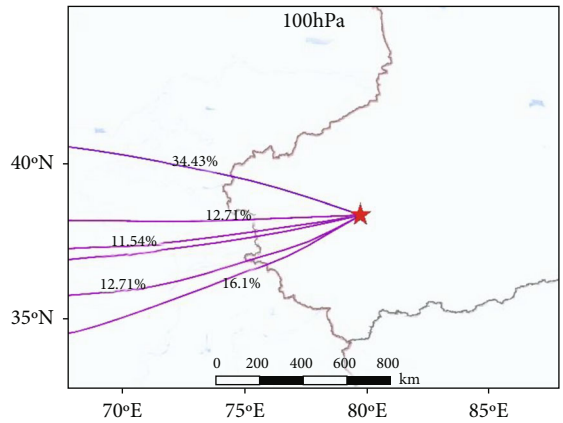

(b) Five-day backward trajectories of the day of maximum gas concentration (February 27)

Figure 10: Backward trajectories in the 100 hPa pressure layer at the gas anomaly center of the Yutian earthquake in 2008. Red five-pointed star indicates the center point of abnormal gas concentration.

gas channels were generally open, and gases were released, resulting in obvious anomalies in March after the earthquake [31].

4.2. Causes of Abnormal TotCO and TotO$_3$. According to previous studies [2, 14, 31], there are currently two primary explanations for the abnormal changes in TotCO and TotO$_3$ in the epicentral area. One explanation is the escape of underground gas along the fault zone, and the other is that the gas dissipating into the atmosphere reacts with original atmospheric gases. However, the contributions of these processes might not be large enough to produce an abrupt increase in total ozone in such a short period [13]. In addition, according to Ganguly [28], atmospheric transportation is also a cause of abnormal changes in TotO$_3$. The causes of abnormal TotCO and TotO$_3$ associated with the two Yutian earthquakes are discussed from these three aspects below.

First, the spatial (Figures 2–5) and temporal (Figures 6, 8, and 9) variations in TotCO and TotO$_3$ anomalies were most likely caused by geological processes in the lithosphere or crustal stress that resulted in the two Yutian M_S7.3 earthquakes in 2008 and 2014. Many gases remain deep in the earth's crust, including CO_2, CO, CH_4, H_2, N_2, H_2O, and H_2S [1]. These gases are stored in the earth's crust at higher than atmospheric pressure, and they tend to migrate upward and penetrate into shallow rock cracks and pores and escape to the atmosphere [15]. During an earthquake, the increase in ground stress causes many cracks, pores, and fissures to form in the fracture zone near the epicenter, and large amounts of carbon-containing gases (e.g., CH_4 and CO) escape into the atmosphere through these channels, causing abnormal changes in gas concentrations in the epicenter area [2]. In this study, the spatial distributions of TotCO and TotO$_3$ corresponded well with the fault zone. However, an earthquake is a complex process, and other factors such as topography, weather, and human activities in the epicenter area can also cause abnormal changes in gas concentrations. In this study, calculations were used during the processing of data to eliminate the influences of other factors, and therefore, underground gas emissions might be the largest cause of abnormal changes in TotCO and TotO$_3$ in the epicenter area.

Second, underground gases escape into the atmosphere and chemically react with atmospheric gases. Gas increments affect atmospheric concentrations in an epicenter area, resulting in abnormal changes in TotCO and TotO$_3$. Following escape from underground, CH4 forms the transition products CO and O_3 during oxidation, according to the

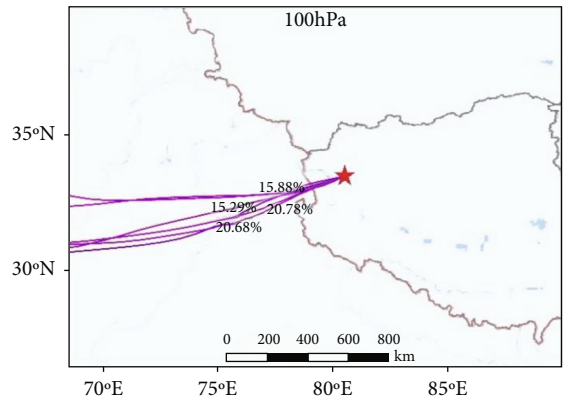

(a) Five-day backward trajectories on the day of the earthquake (February 12)

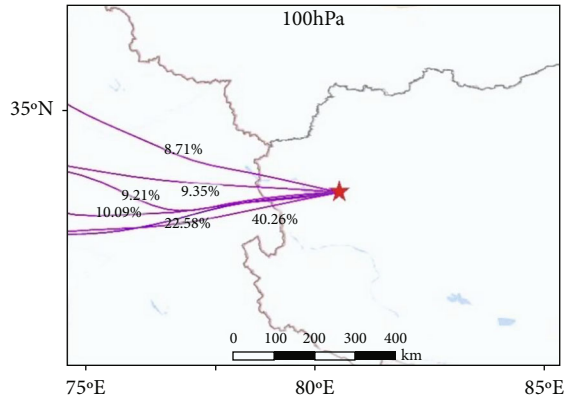

(b) Five-day backward trajectories of the day of maximum gas concentration (March 10)

Figure 11: Backward trajectories in the 100 hPa pressure layer at the gas anomaly center of the Yutian earthquake in 2014. Red five-pointed star indicates the center point of abnormal gas concentration.

reaction $CH_4 + 4O_2 + 2h\nu 1 + h\nu 2 \longrightarrow H_2O + CO + H_2 + 2O_3$, which increases TotCO and $TotO_3$ [32, 33]. Because of the high background content of atmospheric CH_4, the increase in CH_4 from underground gas emissions is limited. Nevertheless, the oxidation of CH_4 contributes to CO and O_3 abnormalities [34–36]. O_3 is distributed primarily in the troposphere, and atmospheric photochemical reactions in the troposphere can also cause abnormal O_3 concentrations, according to the reaction $CO + 2O_2 \longrightarrow CO_2 + O_3$. As shown in Table 2, the coefficients of correlation between CO and O_3 were 0.672 and 0.638 in 2008 and 2014, respectively, with both correlations significant at $p < 0.05$. The correlations between TotCO and $TotO_3$ were relatively weak in 2007, 2009, 2013, and 2015 but were significant in 2008 and 2014, indicating a good correlation between CO and O_3 during an earthquake. Sun et al. [14] studied the changes in TotCO and $TotO_3$ before and after two major earthquakes in Sumatra in 2004 and 2005. They found no correlation between TotCO and $TotO_3$ in 2004 to 2005 ($r = 0.021$), but the correlation was significant during earthquake activity (December 2004 to March 2005) ($r = 0.77$) [14], which is consistent with the results of this study. As shown in Figure 6, the change in $TotO_3$ lagged behind that in TotCO, indicating that the earthquakes caused CO to be oxidized to O_3. The coefficients of correlation between CH_4 and CO in 2008 and 2014 were −0.731 and −0.370, respectively, with correlations significant at $p < 0.05$ and 0.01, respectively. The coefficients of correlation between CH_4 and O_3 in 2008 and 2014 were −0.660 and −0.558, respectively, with both correlations significant at $p < 0.05$, indicating that part of TotCO and $TotO_3$ was also derived from CH_4 oxidation. In addition, during an earthquake, low-frequency electromagnetic radiation and ionospheric disturbances promote 14N decay to form CO [37, 38], accelerating the production of CO according to the reactions $14N(n, p) \longrightarrow 14C + H$ and $2C + O_2 \longrightarrow 2CO$. These reactions are another reason for abnormal changes in TotCO.

Third, atmospheric transmission might also be a cause of abnormal gas concentrations in epicentral areas. The 5-day backward trajectories on the day of the 2008 Yutian earthquake (Figure 10(a)) showed that in the air masses from the NWW direction in the 100 hPa pressure layer, the O_3 contribution rate was the largest at 28.57%. In the remaining air masses, the contribution was relatively small. The 5-day backward trajectories of the maximum O_3 concentration day (Figure 10(b)) showed that the O_3 contribution rate in the air mass from the NWW direction increased to 34.43%. Although the O_3 contribution rate in the other air masses also increased, the magnitude of increase was small. The 5-day backward trajectories on the day of the 2014

Yutian earthquake (Figure 11(a)) showed that among the air masses from the SWW direction, the two air masses closest to the south had the largest contributions of O_3, reaching 20.68% and 20.78%. The 5-day backward trajectories of the day with the maximum O_3 concentration (Figure 11(b)) showed that in the air mass from the SWW direction, the maximum contribution rate of O_3 increased to 40.26%. For the source of the air mass, these results were consistent with those obtained by the difference and abnormal index methods, indicating that atmospheric transportation was also a cause of abnormal changes in $TotO_3$. Ganguly [28] studied the increase in $TotO_3$ after the Gujarat M_S7.7 and M_S5.2 earthquakes in 2001 and 2006, respectively, and found that the increase in $TotO_3$ after the earthquake was due to atmospheric transmission between the upper troposphere and lower stratosphere. The upper O_3-rich air was transported to the epicenter. The results of this study were similar.

5. Conclusions

(1) AIRS hyperspectral remote sensing data were analyzed, and TotCO and $TotO_3$ changed abnormally before and after two M_S7.3 earthquakes in the study area. Abnormal gas concentrations associated with the 2008 Yutian earthquake occurred in February before the earthquake, and those associated with the 2014 Yutian earthquake occurred in March after the earthquake. Before and after the two earthquakes, the anomalies of TotCO and $TotO_3$ were distributed along the fault zone or the anomaly trend was consistent with the fault zone trend.

(2) The release of ground stress during earthquake buildup and occurrence causes the release of underground gases into the atmosphere along the rupture zone, which might be a cause of the abnormal changes in TotCO and $TotO_3$. The CO and O_3 released into the atmosphere chemically react with CH_4 and other original atmospheric gases, which may be another cause of the abnormal changes in TotCO and $TotO_3$. In addition, atmospheric transportation might also contribute to abnormal changes in $TotO_3$.

(3) The abnormal changes in TotCO and $TotO_3$ before and after earthquakes may be anomalies that can predict impending earthquakes. The CO and O_3 anomaly indexes of the two Yutian M_S7.3 earthquakes obtained by the anomaly index method were 2.0 and 2.2 and 2.0 and 2.2, respectively, and the anomaly reliability exceeded 94%. Thus, satellite hyperspectral remote sensing data can be used to extract reliable seismic-related information from geochemical anomalies.

Data Availability

The data are available at http://disc.sci.gsfc.nasa.gov/https://www.noaa.gov/.

Conflicts of Interest

The authors declare that they have no conflicts of interest.

Acknowledgments

The authors are grateful for the financial support from the National Natural Science Foundation of China (Grant No. 41262001).

References

[1] Y. Chen, R. S. Xu, R. Cai, J. Wang, and L. Miao, "Application progress of remote sensing technology in earthquake research," *Progress in Geophysics*, vol. 23, no. 4, pp. 273–1281, 2008.

[2] Y. J. Cui, J. Li, Y. Y. Wang, Y. M. Liu, Z. Chen, and J. G. Du, "Application of gas remote sensing technique to earthquake monitoring," *Advances in Earth Science*, vol. 30, no. 2, pp. 284–294, 2015.

[3] Y. J. Cui, J. G. Du, D. H. Zhang, and Y. T. Sun, "Application of remote gas geochemistry in earthquake prediction," *Advances in Earth Science*, vol. 27, pp. 1173–1177, 2012.

[4] Y. Li, J. G. Du, F. K. Wang, X. C. Zhou, X. D. Pan, and R. Q. Wei, "Geochemical characteristics of soil gas in the Yanhuai basin, northern China," *Earthquake Science*, vol. 22, no. 1, pp. 93–100, 2009.

[5] X. C. Zhou, J. G. Du, Z. Cheng, Y. J. Cui, and L. Liu, "Advance review of seismic geochemistry," *Bulletin of Mineralogy Petrology and Geochemistry*, vol. 31, no. 4, pp. 340–346, 2012.

[6] J. D. Pasteris, "Fluid inclusion in mantle xenoliths," in *Mantle Xenoliths*, pp. 691–707, Wiley, New York, 1987.

[7] J. D. Bergman, "Lamproites and other potassium-rich igneous rocks: a review of their occurrence, mineralogy and geochemistry," in *Alkaline Igneous Rocks*, J. G. Fitton and B. G. J. Upton, Eds., pp. 103–190, Blackwell Scientific Publication, London, 1987.

[8] S. Matveev, C. Ballhaus, K. Fricke, J. Truckenbrodt, and D. Ziegenben, "Volatiles in the Earth's mantle: I. Synthesis of CHO fluids at 1273 K and 2.4 GPa," *Geochimica et Cosmochimica Acta*, vol. 61, no. 15, pp. 3081–3088, 1997.

[9] C. Y. King, "Gas geochemistry applied to earthquake prediction: an overview," *Journal of Geophysical Research: Solid Earth*, vol. 91, no. B12, pp. 12269–12281, 1986.

[10] C. M. Wang and X. H. Li, "Applications of fracture-gas measurement to the earthquake studies in China," *Earthquake Research in China*, vol. 2, pp. 38–53, 1994.

[11] J. G. Du, X. Y. Si, Y. X. Chen, H. Fu, C. L. Jian, and W. S. Guo, "Geochemical anomalies connected with great earthquakes in China," in *Geochemistry Research Advances*, pp. 57–92, Nova Science Publishers, New York, 2008.

[12] X. C. Zhou, J. du, Z. Chen et al., "Geochemistry of soil gas in the seismic fault zone produced by the Wenchuan M_S 8.0 earthquake, southwestern China," *Geochemical Transactions*, vol. 11, no. 1, pp. 1–10, 2010.

[13] N. D. Ganguly, "Variation in atmospheric ozone concentration following strong earthquakes," *International Journal of Remote Sensing*, vol. 30, no. 2, pp. 349–356, 2009.

[14] Y. T. Sun, Y. J. Cui, Y. M. Liu et al., "Anomalies remote sensing geochemistry of CO and O3 and ground-based validation

before and after two Sumatra M>8.0 earthquakes," *Journal of Seismological Research*, vol. 37, no. 2, pp. 222–227, 2014.

[15] Y. J. Cui, D. Ouzounov, N. Hatzopoulos, K. Sun, Z. Y. Zou, and J. du, "Satellite observation of CH_4 and CO anomalies associated with the Wenchuan M_S 8.0 and Lushan M_S 7.0 earthquakes in China," *Chemical Geology*, vol. 469, pp. 185–191, 2017.

[16] R. P. Singh, J. Senthil Kumar, J. Zlotnicki, and M. Kafatos, "Satellite detection of carbon monoxide emission prior to the Gujarat earthquake of 26 January 2001," *Applied Geochemistry*, vol. 25, no. 4, pp. 580–585, 2010.

[17] Z. H. Li, H. S. Ma, and Y. J. Qu, "Study on seismogenic structure and seismic activity characteristics before the Yutian *M*s 7.3 earthquake on March 21, 2008, Xinjiang," *Earthquake Research in China*, vol. 25, no. 2, pp. 199–205, 2009.

[18] H. H. Aumann, M. T. Chahine, C. Gautier et al., "AIRS/AMSU/HSB on the aqua mission: design, science objectives, data products, and processing systems," *IEEE Transactions on Geoscience and Remote Sensing*, vol. 41, no. 2, pp. 253–264, 2003.

[19] B. J. Tian, M. Evan, and F. Eric, *AIRS/AMSU/HSB Version 6 Level 3 Product User Guide*, Jet Propulsion Laboratory and California Institute of Technology, Pasadena, CA, 2014.

[20] G. Rolph, A. Stein, and B. Stunder, "Real-time environmental applications and display system: READY," *Environmental Modelling & Software*, vol. 95, pp. 210–228, 2017.

[21] V. Tramutoli, G. D. Bello, N. Pergola, and S. Piscitelli, "Robust satellite techniques for remote sensing of seismically active areas," *Annals of Geophysics*, vol. 44, no. 2, pp. 295–312, 2009.

[22] D. Ouzounov, D. Liu, K. Chunli, G. Cervone, M. Kafatos, and P. Taylor, "Outgoing long wave radiation variability from IR satellite data prior to major earthquakes," *Tectonophysics*, vol. 431, no. 1-4, pp. 211–220, 2007.

[23] S. J. Nan, M. S. Liang, and J. H. Shi, "Analysis on heavy pollution weather in Taiyuan based on HYSPLIT backward trajectory mode," *Shanxi Science and Technology*, vol. 33, no. 6, pp. 131–133, 2018.

[24] Z. J. Zhao, Y. J. Wei, X. Z. Zhang, W. Qin, and H. F. Xie, "The correlation analysis of Nanjing haze days and meteorological factors," *China Environmental Science*, vol. 35, no. 12, pp. 3570–3580, 2015.

[25] G. H. Yin, J. X. Jiang, and G. D. Wu, "Tectonic background of the *M*s 7.4 earthquake at Yutian on March 21, 2008," *Arid Land Geography*, vol. 31, no. 4, pp. 543–549, 2008.

[26] H. B. Liu, Y. J. Cui, and C. L. Xin, "Detecting anomalies of atmospheric total column CO and O_3 related to the 2014 Yutian *M*s 7.3 earthquake," *Earthquake*, vol. 40, no. 1, pp. 99–111, 2020.

[27] X. Z. Chen, C. S. Jiang, and Y. E. Li, "The March 21, 2008 Yutian, Xinjiang *M*s7.3 earthquake," *Recent Developments in World Seismology*, vol. 4, pp. 20–30, 2008.

[28] N. D. Ganguly, "The impact of transported ozone-rich air on the atmospheric ozone content following the 26 January 2001 and 7 March 2006 Gujarat earthquakes," *Remote Sensing Letters*, vol. 2, no. 3, pp. 195–202, 2011.

[29] Y. G. Wan, Z. K. Shen, and S. Z. Sheng, "The mechanical effects of the 2008 *M*s7.3 Yutian, Xinjiang earthquake on the neighboring faults and its tectonic origin of normal faulting mechanism," *Chinese Journal of Geophysics*, vol. 53, no. 2, pp. 280–289, 2010.

[30] J. J. Ren, X. W. Xu, S. M. Zhang, Y. Luo, O. B. Liang, and J. X. Zhao, "Tectonic transformation at the eastern termination of the Eastern Kunlun fault zone and seismogenic mechanism of the 8 August 2017 Jiuzhaigou M_S7.0 earthquake," *Chinese Journal of Geophysics*, vol. 60, no. 10, pp. 4027–4045, 2017.

[31] H. B. Liu, Y. J. Cui, and C. L. Xin, "Characteristics of CO changes before and after the Yutian *M*s7.3 earthquake in Xinjiang based on AIRS data," *Bulletin of Mineralogy Petrology and Geochemistry*, vol. 39, no. 2, pp. 327–335, 2020.

[32] G. Martinelli and P. Plescia, "Carbon dioxide and methane emissions from calcareous-marly rock under stress: experimental tests results," *Annals of Geophysics*, vol. 48, no. 1, pp. 167–173, 2009.

[33] Q. Y. Yang, Y. Zhang, L. Y. Fu et al., "Coupling mechanism of stress variation and groundwater (water level, water temperature, hydrochemistry, soil gas, etc.) and its application in earthquake precursors research in Sichuan and Yunnan regions," *Progress in Geophysics*, vol. 35, no. 6, pp. 2124–2133, 2020.

[34] B. Weinstock and H. Niki, "Carbon monoxide balance in nature," *Science*, vol. 176, no. 4032, pp. 290–292, 1972.

[35] J. Fishman, S. Solomon, and P. J. Crutzen, "Observational and theoretical evidence in support of a significant in-situ photochemical source of tropospheric ozone," *Tellus*, vol. 31, no. 5, pp. 432–446, 1979.

[36] J. Fishman and W. Seiler, "Correlative nature of ozone and carbon monoxide in the troposphere: implications for the tropospheric ozone budget," *Journal of Geophysical Research Oceans*, vol. 88, no. C6, pp. 3662–3670, 1983.

[37] J. H. Ding, X. H. Shen, W. Y. Pan, J. Zhang, and H. P. Guan, "Seismo-electromagnetism precursor research progress," *Chinese Journal of Radio Science*, vol. 21, no. 5, pp. 791–801, 2006.

[38] X. M. Zhang, J. Liu, J. D. Qian, X. H. Shen, and S. F. Zhao, "Ionospheric electromagnetic disturbance before Gaize earthquake with Ms 6.9, Tibet," *Earth*, vol. 28, no. 3, pp. 14–22, 2008.